Title
6.2 μm spectrum and 6-dimensional morphed potentials of OC-H2O

Authors
Rivera-Rivera, Luis A
McElmurry, Blake A
Scott, Kevin W
et al.

Publication Date
2018-02-01

DOI
10.1016/j.chemphys.2017.11.003

Peer reviewed

6.2 μm Spectrum and 6-Dimensional Morphed Potentials of OC-H_2O

Luis A Rivera-Rivera*, Blake A. McElmurry, Kevin W. Scott, Sean D. Springer,

Robert R. Lucchese, John W. Bevan

Department of Chemistry, Texas A&M University, College Station, TX 77843-3255, USA

Igor I. Leonov

Institute of Applied Physics, Russian Academy of Sciences, Nizhny Novgorod, 603950, Russia

Laurent H. Coudert

Institut des Sciences Moléculaires d'Orsay (ISMO), CNRS, Université Paris-Sud, Univ. Paris-Saclay, 91400 Orsay, France

Abstract

Rovibrational transitions associated with tunneling states in the ν_5 (water bending) vibration of the OC-H_2O complex have been recorded using a supersonic jet mode-hop free quantum cascade laser spectrometer at 6.2 μm. Analysis of the resulting spectra is facilitated by incorporating fits of previously recorded microwave and submillimeter data accounting for Coriolis coupling to confirm assignment of the ν_5 vibration. The theoretical basis of morphing a 5-D frozen monomers potential was initially developed and then extended to two 6-D morphed potentials. A combination of these spectroscopic results and previous rovibrational data for the ν_5 vibration in OC-D_2O are then used to generate a 6-D morphed potential surface for the intermolecular and the water bending vibrations. An alternative 6-D morphed potential of the intermolecular and the

* Present address: Department of Physical Sciences, Ferris State University, Big Rapids, MI 49307-2225. E-mail: LuisRiveraRivera@ferris.edu

ν_3 (CO stretching) vibrations was also generated. These determined morphed potentials then formed the basis for modeling the dynamics of the complex and prediction of accurate intermolecular rovibrational frequencies of the complex.

1. Introduction

While water is the most studied substance, it is remarkable that the science behind its intermolecular interactions with different molecules is frequently relatively poorly understood at the molecular level. An important approach to enhance such understanding is the detailed investigation of prototypical pairwise interactions, which can then provide avenues to greater understanding into properties of water whether in the gas phase or in more complex environments such as in solutions, at interfaces or in solids. OC-H_2O is a pairwise interaction that has received some attention. Water and CO are common and important molecules found in the earth's atmosphere, in the products of combustion reactions and in the interstellar medium, as well as the gas halo of nearby bodies like Europa, one of the satellites of Jupiter, and in comets [1,2]. Consequently, a detailed knowledge of this pairwise interaction can be of considerable significance in modeling a wide range of phenomena. Spectroscopic investigations have provided powerful experimental methods for direct characterizations of such interactions or providing data for correlation with computational approaches.

For the reasons previously discussed, the OC-H_2O complex has been subject of extensive spectroscopic investigations including using high-resolution microwave, submillimeter [3,4], and infrared [5,6] spectroscopies. The latter have included rovibrational analyses of the CO and OH fundamental frequencies in the complex using supersonic jet diode laser absorption spectroscopy [5] and optothermal molecular beam spectroscopy [6] respectively. Extensive investigations of

the complex using infrared matrix isolations spectroscopy have also been completed [7,8]. The complex has, furthermore, been the subject of additional theoretical work [9-18] intended to investigate the potential energy surface of the complex with special reference to its structure and tunneling dynamics as a prototypical system for applicability of different computational methods. Information on the barrier height for interconversion of the two hydrogen atoms has been estimated from a model Hamiltonian to be around 210-230 cm^{-1} from the tunneling splitting in the microwave spectrum [3,4]. The barrier height decreases when the CO stretch is excited, which also weakens the intermolecular bond [5]. The opposite has been found to occur in the O-H asymmetric stretching vibration [6]. However, the multidimensional nature of the tunneling complicates the analysis of the spectra, and the use of a simplified model Hamiltonian, as well as the assumptions made in earlier work that the tunneling splitting is independent of the rotational quantum number K_a, requires further investigation [6].

Recently, we reported a rovibrational analysis of the water bending vibration in the most abundant pairwise complex in the atmosphere, N_2-H_2O [19] using a mode-hop free supersonic jet spectrometer. We now report assignment of the rovibrational transitions associated with tunneling states in the ν_5 (water bending) vibration of the OC-H_2O complex, the vibration associated with the ν_2 bending vibration of the water monomer. This spectrum has been recorded using a mode-hop free supersonic jet quantum cascade laser spectrometer at 6.2 μm [20]. Analysis of the resulting spectra is facilitated by incorporating fits of previously recorded microwave and submillimeter data accounting for Coriolis coupling to obtain the levels of the ground vibrational state. These results are then used to confirm assignment of the ν_5 vibration and to more definitively explore the nature of tunneling dynamics in associated vibrationally excited states of the complex. Furthermore, these and previously available spectroscopic data

including isotopic analyses and an accurate estimate of the D_0 value of OC-H_2O are now included in morphed potential generation of three models: *i*) a 5-D frozen monomer, *ii*) 6-D intermolecular with water bending vibration, and *iii*) 6-D intermolecular with carbon monoxide vibration. The synergistic approach combining high-resolution spectroscopic data with morphing methodologies [21-25] has now advanced significantly giving a powerful method for describing unexpected intrinsic properties in intermolecular interactions. Recently, a 6-D vibrationally-complete semi-empirical electronic ground state potential has been generated for the hydrogen-bonded dimer OC-HF through application of a morphing methodology [25]. The intention of this previous work has been to develop a generalized methodology that transforms initially inaccurate *ab initio* potential functions to morphed potentials capable of enhanced predictive accuracy for non-covalent interactions. The development of compound-model morphing approach with radial shifting (CMM-RS) for OC-HF was facilitated by an adiabatic separation of intramolecular vibrations of the complex from the low frequency intermolecular vibrations. Four parameterized morphing coefficients only were used to correct for basis set superposition and electron correlation errors while scaling of the potential and shifting of its minimum compensated for inadequacies in the underlying *ab initio* potential. The morphing transformation utilized a rotationally resolved spectroscopic database composed of microwave and infrared spectroscopic information. Morphing was completed to near spectroscopic accuracy for available rotationally and rovibrationally analyzed spectroscopic data with wavelengths greater than 2.5 μm not demonstratively affected by perturbations outside the model methodology. Band origin vibrational frequencies were fitted to an unprecedented average standard deviation of 0.016 cm^{-1} while rotational constants were determined to 1-2 parts in 10^4 for the database. It is now important to critically and quantitatively evaluating the predictive capability of this CMM-RS

methodology but to also to apply the methodology to more general pairwise molecular complexes in particular OC-H_2O, a prototype water complex. In the current work, we shall develop algorithms for the 5-D and 6-D morphed potentials for OC-H_2O. These model results will be compared with the previously available spectroscopic data and also used to make predictions of the rovibrational data for the intermolecular vibrations based on the current available spectroscopic analyses and an accurate estimate of the ground state dissociation energy [26].

2. Experimental Methods

The cw slit jet infrared quantum cascade laser (QCL) spectrometer used in the current investigations is based on a similar design to that of a previously constructed lead salt continuous slit jet semiconductor laser spectrometer [27] but with accommodations necessary for substitution of quantum cascade lasers (QCLs) as sources [28]. The quantum cascade laser (QCLs) employed in the current investigations were fabricated by Daylight Solutions (San Diego, California) and have mode-hop free operational ranges from 1570 to 1640 cm^{-1} (21045-MHF). Details of the QCL spectrometer have been given elsewhere [28], thus only a short description of the instrument will be given in this work. The laser controllers were connected via GPIB interface to the host computer and the output frequency and power of the laser head could be set by a custom LabVIEW program with integrated VI's from the manufacturer. Tuning of the output frequency of the QCL head can be achieved by two methods. Coarse tuning of the output frequency determined by controlling a stepping motor that changes the QCL cavity length through a pivoted external cavity grating while sustaining a single cavity mode. Laser output powers in the range 80-100 mW are typical once threshold emission had been achieved.

Wavelength modulation of the laser source was achieved by the application of a sinusoidal waveform with a frequency of 10 kHz to 2 MHz (MF) and a modulation amplitude, MA, of ±2 V DC giving up to 0.05 cm^{-1} modulation amplitude in frequency. Frequency tunability and single mode-hop free operation was characterized to have a free-running linewidth of <20 MHz. The output of the laser was first split by a CaF_2 wedge and following redirection by a reflection mirror, split again into three components using CaF_2 beam splitters. The transmitted beam from the first CaF_2 beam splitter was collected by a Wood's horn to reduce back reflections and eliminate feedback to the QCL chip. The total power used in the current experiment is estimated to be about 0.8 mW. The detectors used in the current study were LN_2 cooled MCT detectors (Graesby Infrared or Infrared Associates) and preamplifiers having a 1 MHz bandwidth. The output of these detectors were sampled by three EG&G 5302 lock-in amplifiers referenced to the modulation signal. The output of the lock-in amplifiers were digitized and stored in the computer using the LabVIEW program and DAQ interface. The absolute frequency scale of the observed spectrum was determined by a combination of passive Fabry-Perot confocal etalon (Spectra-Physics, SP5945) with a FSR of 0.00962456 cm^{-1} referenced to carbon monoxide (1 Torr, 30 cm path) and nitrous oxide (10 Torr, 10 cm path) standard transitions from the HITRAN database that were used for calibration of absolute frequencies to an accuracy of ±0.0005 cm^{-1}. The 12 cm long slit jet expansion was formed from a reservoir sample maintained at a total pressure in the range 15-30 psi consisting of typically 5% carbon monoxide mixed with 94% argon carrier bubbled through a water reservoir and spectra recorded with single pass of the radiation source through the supersonic jet expansion. The vacuum chamber housing the slit expansion was pumped to 600 mTorr by a Leybold RA2001 Roots blower and a Leybold SV630F roughing pump.

3. Theoretical Methodology

i) *Ab initio* calculations of the interaction potentials

Figure 1 illustrates the coordinates system use in this work for OC-H_2O complex. R is the distance between the center of mass of water and CO molecules. The CO and OH bond lengths are described by r_{CO} and r_{OH}. The angles θ_1 and θ_2 describe the orientation of the interacting monomers relative to the line containing the center of masses. χ describe the water rotations on its C_{2v} axis. The angle H-O-H is described by θ_{HOH} and the dihedral angle ϕ describes the relative internal orientation of the monomer components.

Non-relativistic *ab initio* interaction energies of the complex were calculated using the MOLPRO 2010 electronic structure packages [29]. The augmented correlation consistent polarized valence N-ζ basis set (aug-cc-pVNZ) was used, where N represents triple (T) and quadruple (Q) functions [30-32]. The calculated *ab initio* potentials are: (*i*) coupled cluster singles and doubles with perturbative triples (CCSD(T)/aug-cc-pVTZ) and (*ii*) Moller-Plesset second order (MP2/aug-cc-pVNZ). All the interaction energies were then corrected for the basis set superposition error (BSSE), using the counterpoise (CP) method of Boys and Bernardi [33]. Also, the CCSD(T)/aug-cc-pVTZ potential without the CP correction was calculated.

ii) Fitting of the *ab initio* potentials

The full 9-D potential for OC-H_2O system is given by

$$V\left(R,r_{OH},r_{OH},r_{CO},\theta_{HOH},\theta_1,\theta_2,\phi,\chi\right)=V^{int}\left(R,r_{OH},r_{OH},r_{CO},\theta_{HOH},\theta_1,\theta_2,\phi,\chi\right)+V_{H_2O}\left(r_{OH},r_{OH},\theta_{HOH}\right)+V_{CO}\left(r_{CO}\right) \quad (1)$$

In this work, both O-H bonds lengths were frozen to 0.9753 Å, thus Eq. (1) is reduced to 7-D and $V^{int}\left(R,r_{CO},\theta_{HOH},\theta_1,\theta_2,\phi,\chi\right)$ is a 7-D *ab initio* interaction potential. The water molecule potential

was taken from the literature [34] and was evaluated at the fixed r_{OH} values as $V_{H_2O}\left(\theta_{HOH}\right)$. The CO potential, $V_{CO}\left(r_{CO}\right)$, was taken to be the CO RKR potential [35]. The CO RKR potential was fitted to Morse expansion (with $N = 18$) as [36]

$$V_{CO}\left(r_{CO}\right)=\sum_{s=0}^{N}\left[B_s\left(1-e^{-\beta\left(r_{CO}-r_{CO,e}\right)}\right)^s\right] . \tag{2}$$

In order to have a global representation of the interaction potential, the calculated *ab initio* points, at each value of R_i, $r_{CO,j}$, and $\theta_{HOH,k}$ were fitted to the spherical expansion [37,38]

$$V_A^{int}\left(R_i,r_{CO,j},\theta_{HOH,k},\theta_1,\theta_2,\phi,\chi\right)=\sum_{\Lambda}v_{\Lambda,i,j,k}\left(\theta_1,\theta_2,\phi,\chi\right)A_\Lambda\left(\theta_1,\theta_2,\phi,\chi\right). \tag{3}$$

In Eq. (3) Λ is a collective symbol for the quantum numbers (L_1,K_1,L_2,L), $v_{\Lambda,i,j,k}\left(\theta_1,\theta_2,\phi,\chi\right)$ are the expansion coefficients and $A_\Lambda\left(\theta_1,\theta_2,\phi,\chi\right)$ are the expansion angular functions [39]. The interaction potential in Eq. (3) would be the same as the one in Eq. (1) if R, r_{CO}, and θ_{HOH} coordinates had been interpolated. The expansion coefficients $v_{\Lambda,i,j,k}\left(\theta_1,\theta_2,\phi,\chi\right)$ are evaluated by an interpolating moving least-squares procedure [40], by minimizing

$$I=\sum_{\varsigma}W_\varsigma\left(\theta_1,\theta_2,\phi,\chi\right)\left[\begin{matrix}V^{int}\left(R_i,r_{CO,j},\theta_{HOH,k},\theta_{1,\varsigma},\theta_{2,\varsigma},\phi_\varsigma,\chi_\varsigma\right)\\-\sum_{\Lambda}v_{\Lambda,ijk}\left(\theta_1,\theta_2,\phi,\chi\right)A_\Lambda\left(\theta_{1,\varsigma},\theta_{2,\varsigma},\phi_\varsigma,\chi_\varsigma\right)\end{matrix}\right]^2 . \tag{4}$$

In Eq. (4) $W_\varsigma\left(\theta_1,\theta_2,\phi,\chi\right)$ is the weight function of the *ab initio* points in the fitting and is given by

$$W_\varsigma\left(\theta_1,\theta_2,\phi,\chi\right)=\frac{\exp\left(-\alpha d_\varsigma^2\right)}{\left(d_\varsigma^n+\varepsilon\right)}, \tag{5}$$

where the parameters α and n control the rate of attenuation of the weight function, and ε remove the singularity which occurs as $d_\varsigma \to 0$. In Eq. (5) d_ς is the Euclidean distance function given by

$$d_\varsigma\left(\theta_1,\theta_2,\phi,\chi\right)=\sqrt{\begin{array}{l}\left(\theta_1-\theta_{1,\varsigma}\right)^2+\left(\theta_2-\theta_{2,\varsigma}\right)^2+\min\left[\left(\phi-\phi_\varsigma\right)^2,\left(2\pi-\left|\phi-\phi_\varsigma\right|\right)^2\right]\\ +\min\left[\left(\chi-\chi_\varsigma\right)^2,\left(2\pi-\left|\chi-\chi_\varsigma\right|\right)^2\right]\end{array}}. \qquad (6)$$

In order to speed the interpolation and reduced the computational cost, points with $W_\varsigma < 0.01$ were not included on the least-squares fitting procedure.

The radial potential is obtained by interpolating the angular potential on the grid of R_i points, at each value of $r_{\mathrm{CO},j}$, and $\theta_{\mathrm{HOH},k}$ at fixed angular coordinates, using a 1-D radial reproducing kernel of the form

$$V_\Omega^{\mathrm{int}}\left(R,r_{\mathrm{CO},j},\theta_{\mathrm{HOH},k},\theta_1,\theta_2,\phi,\chi\right)=\left(\left|V_{\min}\right|+V_{\mathrm{M}}\right)\left[\exp\left(\sum_i \alpha_{i,j,k}\left(\theta_1,\theta_2,\phi,\chi\right)\, q_1^{2,3}\left(R_i,R\right)\right)-1\right]. \qquad (7)$$

In Eq. (7), $\left|V_{\min}\right|$ represents the absolute value of the minimum of $V_{\mathrm{A}}^{\mathrm{int}}\left(R,r_{\mathrm{CO},j},\theta_{\mathrm{HOH},k},\theta_1,\theta_2,\phi,\chi\right)$, defined as in Eq. (3), and V_{M} is a real positive parameter. The function $q_1^{2,3}$ in Eq. (7) is a 1-D radial reproducing kernel [41].

At each value of the 5-D grid $\left(R,\theta_1,\theta_2,\phi,\chi\right)$, the final interpolated potential is then given by

$$V^{\mathrm{int}}\left(R,r_{\mathrm{CO}},\theta_{\mathrm{HOH}},\theta_1,\theta_2,\phi,\chi\right)=\sum_{jk} C_{jk}\left(R,\theta_1,\theta_2,\phi,\chi\right)Q_{jk}\left(r_{\mathrm{CO},j},\theta_{\mathrm{HOH},k}\right), \qquad (8)$$

where the indexes j and k run over the interpolated $r_{\mathrm{CO},j}$ and $\theta_{\mathrm{HOH},k}$ points. The interaction potential in Eq. (8) is the same to that in Eq. (1) with frozen O-H bonds length. The expansion coefficients $C_{jk}\left(R,\theta_1,\theta_2,\phi,\chi\right)$ are obtained by simple matrix multiplication

$$C_{jk}\left(R,\theta_1,\theta_2,\phi,\chi\right)=\sum_{j'k'}Q_{jk}\left(r_{\mathrm{CO},j'},\theta_{\mathrm{HOH},k'}\right)V_{\Omega}^{\mathrm{int}}\left(R,r_{\mathrm{CO},j'},\theta_{\mathrm{HOH},k'},\theta_1,\theta_2,\phi,\chi\right), \tag{9}$$

due to the orthogonality of the fitting functions. The interaction potential in Eq. (9) is defined in Eq. (7). The 2-D orthogonalized fitting functions, $Q_{jk}\left(r_{\mathrm{CO},j},\theta_{\mathrm{HOH},k}\right)$, for the r_{CO} and θ_{HOH} coordinates used in Eqs. (8) and (9) are defined by [42]

$$Q_{jk}\left(r_{\mathrm{CO}},\theta_{\mathrm{HOH}}\right)=\overline{q}_{2,j}^{2}\left(Z_{\mathrm{CO}}\right)\overline{q}_{2,k}^{2}\left(Z_{\mathrm{HOH}}\right). \tag{10}$$

In Eq. (10), the $\overline{q}_2^2$ are the orthogonalized angle-like reproducing kernel [41], and the function Z is defined by

$$Z_{\mathrm{CO}}\left(r_{\mathrm{CO}}\right)=\frac{\left(r_{\mathrm{CO}}-r_{\mathrm{CO,start}}\right)}{\left(r_{\mathrm{CO,end}}-r_{\mathrm{CO,start}}\right)} \tag{11a}$$

$$Z_{\mathrm{HOH}}\left(\theta_{\mathrm{HOH}}\right)=\frac{\left(\theta_{\mathrm{HOH}}-\theta_{\mathrm{HOH,start}}\right)}{\left(\theta_{\mathrm{HOH,end}}-\theta_{\mathrm{HOH,start}}\right)}. \tag{11b}$$

***iii*) Use of the vibrational adiabatic approximation**

In order to simplify the 7-D potential, we considered two 6-D potentials by fixing the r_{CO} or the θ_{HOH} coordinate. These 6-D potentials where further simplified to 5-D potentials by separated the r_{CO} or the θ_{HOH} coordinates from the bending and stretching motions of the complex using vibrational self-consistent-field (VSCF) calculations [43]. By carrying out these approximations, the 6-D potentials becomes $V^{\upsilon_{\mathrm{X}}}\left(R,\theta_1,\theta_2,\phi,\chi\right)$ [42], (υ_{X} is the vibrational quantum number for the CO stretch or the water bend), which represents the intermolecular potential of the complex averaged over the CO or water bend vibrational states.

In the VSCF a basis set of eigenfunctions of the free monomers are used. The eigenfunctions for the CO stretching are obtained from the solution of the radial Schrödinger equation, which is

solved using a modified Numerov-Cooley approach [25,44]. For the water bending the eigenfunctions are obtained by solving the free water Hamiltonian [45] with frozen O-H bonds on particle in the box eigenfunctions. The VSCF calculations were sped up by pre-calculating all the integrals and matrix elements needed in the calculation. This was achieved by evaluating the integral of the fitting functions in r_{CO} and θ_{HOH} coordinates over the free monomers eigenfunctions. These integrals were evaluated using the extended Simpson's rule [46].

***iv*) Solving the 5-D intermolecular problem**

The simplification of the 6-D potential to a 5-D by adiabatically separating the monomer vibration from the bending and stretching motions of the complex, greatly reduces the computational effort required to complete the rovibrational energy calculations. Within this approximation, the rovibrational Hamiltonian becomes [39,47]

$$H = T_1 + T_2 + \frac{1}{2\mu_{1,2}R^2}\left[-\hbar^2\frac{\partial}{\partial R}R^2\frac{\partial}{\partial R} + J^2 + j_{1,2}^2 - 2\mathbf{j}_{1,2}\cdot\mathbf{J}\right] + V^{\upsilon_X}\left(R,\theta_1,\theta_2,\phi,\chi\right), \qquad (12)$$

where the H_2O and CO monomers are labeled 1 and 2, respectively. In Eq. (12) $\mu_{1,2}$ is the reduced mass of the complex, T_i and $\mathbf{j}_i$ (i = 1 and 2) are respectively the rotational Hamiltonian and angular momentum of monomer i, $\mathbf{J}$ is the total angular momentum, and $\mathbf{j}_{1,2} = \mathbf{j}_1 + \mathbf{j}_2$. Thus, the rovibrational energy levels can be calculated using the pseudo-spectral approach discussed previously [25,48,49].

***v*) Compound model morphing method with radial correction**

In the compound model morphing method with radial correction (CMM-RC), the potential is generated as

$$
\begin{aligned}
V_{\text{CMM-RC}}(R) = {} & C_1\left[V_{\text{MP2}}(R')\right]_{\text{QZ}}^{\text{CP}} + C_2\left\{\left[V_{\text{CCSD(T)}}(R')\right]_{\text{TZ}}^{\text{CP}} - \left[V_{\text{CCSD(T)}}(R')\right]_{\text{TZ}}^{\text{NO CP}}\right\} \\
& + C_3\left\{\left[V_{\text{CCSD(T)}}(R')\right]_{\text{TZ}}^{\text{CP}} - \left[V_{\text{MP2}}(R')\right]_{\text{TZ}}^{\text{CP}}\right\} \qquad , \qquad (13) \\
R' = {} & C_4\left(R - R_{\text{f}}\right) + \left(1.0 + C_5\right)R_{\text{f}}
\end{aligned}
$$

where the C_α are the unitless morphing parameters. The reference or unmorphed potential, $V_{\text{CMM-RC}}^{(0)}$, is obtain by initially choosing C_1 = 1.0, C_2 = 0.0, C_3 = 1.0, C_4 = 1.0, and C_5 = 0.0. The morphing parameters C_α are determined by using a regularized nonlinear least-squares optimization [50]. In Eq. (13), the parameter C_1 is the scaling parameter for the interaction energy of the dimer at the MP2/aug-cc-pVQZ level of theory including the CP correction for the BSSE. The second term in Eq. (13) corrects for BSSE at the CCSD(T) level of theory, while the third term contributes corrections for the correlation energy at the CCSD(T) level of theory. Lastly, the radial correction is included with the parameter C_4 and C_5. It is noted that the potentials functions in Eq. (13) depend on all vibrational coordinates (see Fig. 1) that are taking into consideration during the morphing procedure. For clarity, only the R dependence is explicitly shown in Eq. (13).

***vi*) Details of the Calculations**

The four *ab initio* potentials calculated for the OC-H_2O complex and used to construct the CMM-RC potentials in the current work are: (i) CCSD(T)/aug-cc-pVTZ, (ii) MP2/aug-cc-pVQZ, (iii) MP2/aug-cc-pVTZ, and (iv) CCSD(T)/aug-cc-pVTZ without the CP correction. Two sets of these four *ab initio* potentials were calculated in a 6-D grid of: (*i*) 560,000 $\left(R, r_{\text{CO}}, \theta_1, \theta_2, \phi, \chi\right)$ points, and (*ii*) 336,000 $\left(R, \theta_{\text{HOH}}, \theta_1, \theta_2, \phi, \chi\right)$ points.

For the two sets of *ab initio* potentials the R distance was varied by using a ten-point grid (3.50, 3.75, 4.00, 4.25, 4.50, 4.75, 5.00, 5.50, 6.00, and 7.00 Å); the angles θ_1 and θ_2 were varied

by using a ten-point grid (5.0, 10.0, 15.0, 40.0, 80.0, 100.0, 140.0, 165.0, 170.0, and 175.0 degrees); the dihedral angle ϕ was varied by using an eight-point grid (0.0, 45.0, 90.0, 135.0, 180.0, 225.0, 270.0, and 315.0 degrees); the angle χ was varied by using a twelve-point grid (0.0, 10.0, 50.0, 90.0, 130.0, 170.0, 180.0, 190.0, 230.0, 270.0, 310.0, and 350.0 degrees). Additional points obtained by symmetry include $\phi = 0.0°$ and 180.0°, $\chi = 360°\text{-}\chi$ (for $\chi \neq 0.0°$, 90.0°, 180.0°, and 270.0°) for all R, θ_1, and θ_2 values. These generate a 5-D grid of 112,000 $\left(R,\theta_1,\theta_2,\phi,\chi\right)$ points for a fix r_{CO} and θ_{HOH} value. For the 5-D potentials used in the morphing procedure r_{CO} = 1.1283 Å and θ_{HOH} = 104.0°. For the 6-D potentials involving the r_{CO} coordinate, the θ_{HOH} coordinate was fixed to 104.0°, and the CO bond length, r_{CO}, was varied by using a five-point grid (1.0071, 1.0534, 1.1283, 1.2196, and 1.2995 Å). For the 6-D potentials involving the water bending, the r_{CO} coordinate was fixed to 1.1283 Å, and the H-O-H angle, θ_{HOH}, was varied by using three-point grid (94.0°, 104.0°, and 114.0°).

Parameters α, n, and ε in Eq. (5) were chosen to be 0.80 radians^{-2}, 4, and 10^{-12} radians^4 respectively. The parameter V_M in Eq. (7) was chosen to be 300 cm^{-1}. The values of α, n, ε, and V_M are adjusted to obtain the smoothest fit. The convergence of the adiabatic potential and rovibrational energy calculations depends on the selection of the following parameters: R_{start} = 3.50 Å (the first point of the R radial grid), R_{end} = 7.00 Å (the last point of the R radial grid), $r_{CO,start}$ = 0.90 Å (the first point of the r_{CO} radial grid), $r_{CO,end}$ = 1.40 Å (the last point of the r_{CO} radial grid), $\theta_{HOH,start}$ = 94.0° (the first point of the θ_{HOH} angular grid), $\theta_{HOH,end}$ = 114.0° (the last point of the θ_{HOH} angular grid), N_R = 54 (the number of grid points in the R radial direction), $N_{r_{CO}}$ = 701 (the number of grid points in the r_{CO} radial direction), $N_{\theta_{HOH}}$ = 101 (the number of grid points in the θ_{HOH} angular grid), the number of particle in the box eigenfunctions used was

11, $N_{\theta_1} = N_{\theta_2} = 20$ (the number of θ_1 and θ_2 points used in the grid), $N_\phi = 36$ (the number of ϕ points used in the grid), and $N_\chi = 36$ (the number of χ points used in the grid). The number of radial spectral basis functions is $N_F = 50$. All of the summations over spectral states are truncated so that $k_{\max_1} = j_{\max_1} = 16$, $j_{\max_2} = 16$, include all possible values of m_1 and m_2. The tolerance (τ_L) used to determine the convergence of the eigenvalues in the Lanczos procedure [51] was 10^{-12} atomic units. In the VSCF calculation the number of basis set function used for the adiabatic potential in the CO stretching vibration was 4, and for the adiabatic potential in the water bending was 3. For the kinetic energy operator T_1 and T_2 in Eq. (12) the free monomers rotational constants in the ground and excited vibrational sates were used [52-56]. Lastly, in Eq. (13) the value of R_f was chosen to be 4.00 Å.

4. Spectral Analysis

The tunneling splitting in the ground state of the OC-H_2O complex is due to a large amplitude motion (LAM) involving a planar rotation of the water moiety about its *c*-axis through an angle γ_{LAM} close to 104.5°. This LAM exchanges the hydrogen atoms of the water moiety and also takes place in the $v_5 = 1$ excited vibrational state involved in the present data set.

OC-H_2O displays two equilibrium configurations which in Fig. 5 of Leung *et al.* [57] can be taken as configurations 1 and 3. This numbering will be adopted in the present work and, just as in this figure, the two hydrogen atoms of the water moiety will be labeled 1 and 2. The permutation-inversion symmetry group [58] to be used for the complex is the order 4 commutative group G_4 containing the identity E, the permutation (12) of the two water molecule hydrogen atoms, the inversion E^*, and their product (12)*. The character table of G_4 can be found in Table I. As in Coudert and Hougen [59], the Hamiltonian matrix is setup with the help

of rovibrational basis set wave functions written:

$$\Psi_{1JK\alpha} = \psi_1 \cdot |J, K, \alpha > \quad \text{and} \quad \Psi_{3JK\alpha} = \psi_3 \cdot |J, K, \alpha >, \tag{14}$$

where ψ_1 and ψ_3 are reference framework functions for configurations 1 and 3, respectively; and $|J, K, \alpha >$ is the Wang combination defined in Eq. (1) of Coudert *et al.* [60]. These rotational functions can be characterized by their symmetry species in C_s which is A' or A'' depending on whether $\alpha(-1)^{J+K}$ is +1 of -1. Symmetry adapted wave functions are built using the wave functions in Eqs. (14) and are characterized by their symmetry species in G_4 and the C_s symmetry of the rotational function. This allows us to split the Hamiltonian matrix into four submatrices. Matrix elements of the rotational Hamiltonian H_R and of the tunneling Hamiltonian between two $|J, K', \alpha' >$ and $|J, K'', \alpha'' >$ Wang-type rotational functions arise for each submatrix and can be found in Table II. The matrix elements of the tunneling Hamiltonian, denoted $H_{1JK';3JK''}$ in agreement with the IAM treatment of Hougen [61] and Coudert and Hougen [59], are non-vanishing when both rotational functions belong to the same C_s symmetry:

$$H_{1JK';3JK''} = h_3(-1)^{K'}\left[d^{(J)}(\theta_3)_{K',K''} + \alpha'' d^{(J)}(\theta_3)_{K',-K''}\right], \tag{15}$$

where h_3, with $h_3 < 0$, is the magnitude of the tunneling splitting and θ_3 is an angle which, in the IAM treatment [59,61], describes the rotational dependence of the tunneling splitting. This angle can be evaluated using Eqs. (49) of Hougen [61]. Due to the planar nature of the present LAM, an approximate expression for θ_3 can be retrieved:

$$\theta_3 = \gamma_{\text{LAM}} \frac{C(\text{OC-H}_2\text{O})}{C(\text{H}_2\text{O})}, \tag{16}$$

where $C(\text{CO-H}_2\text{O})$ and $C(\text{H}_2\text{O})$ are the C rotational constants of the water moiety and of the complex, respectively. Taking $\gamma_{\text{LAM}} = 104.5°$, Eq. (16) yields $\theta_3 = 1.032°$ or 0.0180 rad. The angle θ_3 is therefore small and this allows us to approximate the expression of the tunneling

matrix element in Eq. (15) by:

$$H_{1JK';3JK''} = h_3(-1)^{K'}\delta_{K',K''}, \quad (17)$$

where $\delta_{K',K''}$ is the Kronecker δ function. This equation and Table II lead to a rotational-tunneling energy equal to:

$$E_R(JK_aK_c) \pm (-1)^{K_a}h_3, \quad (18)$$

where the first term is the pure rotational energy of a JK_aK_c rotational level and the upper (lower) sign should be used for $A^{\pm}$ ($B^{\pm}$) symmetry species. The corresponding energy level diagram can be found in Fig. 1 of Bumgarner *et al*. [4]. This figure emphasizes that tunneling from $K_a = 0$ and 1 leads to $A^{\pm}$ and $B^{\pm}$ sublevels, the former being below the latter for $K_a = 0$ while it is the opposite for $K_a = 1$. These results are consistent with selection rules for ΔK_a=0, *a*-type transitions being bottom to bottom (b-b) and top to top (t-t) while those for ΔK_a=1 *b*-type transitions will be bottom to top (b-t). In Bumgarner *et al.* [4], tunneling sublevels were identified using a torsional quantum number ν_t such that $A^{\pm}$ and $B^{\pm}$ sublevels correspond respectively to ν_t = 0 and 1 for K_a=0; and ν_t = 1 and 0 for K_a=1. When expressed with this labeling scheme, selection rules for *a*- and *b*-type transitions are then $\Delta\nu_t$ = 0 and $\Delta\nu_t$ = 1, respectively.

5. Results and Discussion

Spectra of the H_2O bending in OC-H_2O were recorded using a highly sensitivity QCL cw supersonic jet spectrometer at 6.2 μm. Figure 2 show the assigned spectrum of the Σ←Σ rovibrational transition over the frequency range 1599.0 to 1600.8 cm^{-1}. The effective resolution of the spectrum is 80 MHz (0.003 cm^{-1}). Figure 3 show the QCL cw supersonic jet spectrum of a segment of the Π←Σ transition in OC-H_2O in the frequency range 1618.0 to 1619.8 cm^{-1}. The

spectrum shows transitions involving the A and B states in OC-H_2O. A segment of the Ar-H_2O complex is apparent at 1618.5 cm^{-1}. The observed $K = 0 \leftarrow 0$ and $K = 0 \leftarrow 1$ transitions of OC-H_2O are given, respectively, in Tables III and IV. The corresponding spectroscopic constants are given in Tables V and VI.

A weighted least-squares fit of the *a*- and *b*-type microwave transitions reported by Yaron *et al.* [3] and Bumgarner *et al.* [4]; and of the *a*- and *b*-type transitions measured in this work was carried out. In the least-squares fit procedure, for the ground and $v_5 = 1$ states, rotational and distortion constants were varied along with the tunneling parameters h_3, θ_3 of Eq. (15) and the distortion tunneling parameters h_{3K}, h_{3J}, f_3, h_{3KJ}, h_{3JJ}, and f_{3J}, defined as in Coudert *et al.* [60]. Parameters are listed in Table VII. The value of 1.5 obtained for the unitless standard deviation is satisfactory and seems to indicate that the present assignments are correct. This is confirmed by the somewhat agreement between the value of θ_3 calculated with Eq. (16) and that retrieved from the fit. Due to the magnitude of the tunneling splitting as defined in Eq. (15), the sub-band center difference of the tunneling components of the infrared sub-bands is twice the difference between the h_3 parameters of the ground and $v_5 = 1$ states, that is 0.16 cm^{-1} as can be gathered from Table VII.

The potential morphing methodology developed in this work allows the generation of a 7-D morphed potential for the OC-H_2O complex that include the CO stretching and the water bend. However, due to limitations of the interpolating moving least-squares procedure, such calculations are not feasible with available computer resources. We have then generated three different morphed potentials for the OC-H_2O complex namely: a 5-D potential, $\left(V^{(5)}_{\text{5-D,CMM-RC}}\right)$, where both monomer are frozen; a 6-D potential, $\left(V^{(5)}_{\text{6-D,HOH,CMM-RC}}\right)$, with the CO monomer frozen

and only the bend is considered in the water monomer; and a 6-D potential, $\left(V^{(5)}_{\text{6-D,CO,CMM-RC}}\right)$, where the water monomer is frozen and the CO stretching is considered. The experimental data used to morph the intermolecular potentials energy surfaces are presented in Tables VIII to X. The RMS of the fits indicates the improvement in the overall agreement with experiment obtained from the morphing procedure. The final morphing parameters, which yielded the best fits to the experimental data, are given in Table XI.

Table XII gives prediction of the water bending in the complex, based on the 6-D water bending CMM-RC potential $\left(V^{(5)}_{\text{6-D,HOH,CMM-RC}}\right)$. The small deviation of the predicted data on third column of Table XII is a consequence of structural changes of the water monomer on complexation and couplings among intra- and inter-molecular vibrations. The current model does not take in consideration such effects since both O-H bonds in the water monomer are held frozen. In order to account to such effects a 9-D morphed potential will be required, but it is not at the reach of current computational capabilities. To partially correct such effects, we apply corrections to the kinetic energy of the water monomer. The rotational constant A for the free monomer in the excited sate was increase by 0.93 cm^{-1} in H_2O and by 0.38 cm^{-1} in D_2O. In addition the mass of one of the hydrogen (deuterium) atom was reduced by 0.1 u in H_2O and by 0.09 u in D_2O. The predictions based on these corrections are given on the fourth column of Table XII.

Predictions of fundamental intermolecular vibrational frequencies for OC-H_2O are given in Table XIII. The assignment of the intermolecular frequencies is as follows. ν_9 and ν_8 are the lower frequency bending modes; the ν_9 vibration is in the complex plane and the ν_8 vibration is out of the plane. ν_4 is the intermolecular stretch vibration. Due to complexity of the rovibrational

wave function, we cannot definitely predict the two higher frequency bending modes of the complex. Further experimental studies are needed.

Prediction of D_0 for OC-H_2O was estimated to be 355(13) cm^{-1} bases on applications of potential morphing to the Badger-Bauer rule [26]. As show in Table XIV the D_0 predictions of the current morphed potentials range from 337(5) to 342(5) cm^{-1} for OC-H_2O and from 389(6) to 394(6) cm^{-1} for OC-D_2O. The morphed potential predictions for D_0 agree within the error bars to the Badger-Bauer rule predictions, given a validation of predicted capabilities of the Badger-Bauer rule derived from potential morphing [26].

The predicted tunneling splitting in the $K = 0$ ground vibrational state base on the morphed potentials is 0.83 cm^{-1} for OC-H_2O and 0.04 cm^{-1} for OC-D_2O. These values compare with the values of 0.557 cm^{-1} for OC-H_2O and 0.034 cm^{-1} for OC-D_2O calculated by Bumgarner *et al.* [4] assuming that the tunneling splitting is the same in the $K = 0$ and $K = 1$ states. The discrepancy in these values can be attribute to the fact that the tunneling splitting has a dependence on the quantum number K [62]. Oudejans and Miller [6] calculated the tunneling splitting in the $K = 1$ ground vibrational state of OC-H_2O to be 0.304 cm^{-1} in agreement with our prediction of 0.27 cm^{-1}.

The left panels of Fig. 4 show 2-D slices of the CMM-RC interaction potentials of OC-H_2O. The corresponding estimated errors relative to the potential at infinite separation are shown in the right panels. Panels A and D correspond to the 5-D frozen monomer CMM-RC potential. Panels B and E and panels C and F correspond, respectively, to the adiabatic 6-D CMM-RC potential in the vibrational ground state of the water bending and the CO stretching. In the three cases the potential surface have two equivalent global minima (due to the tunneling dynamics of the hydrogen atoms) locate at $R = 3.97$ Å, $\theta_1 = 125.0°$, $\theta_2 = 180.0°$, and $\phi = \chi = 0.0°$; and $R = 3.97$ Å,

θ_1 = 235.0°, θ_2 = 180.0°, and $\phi = \chi$ = 0.0°. The predicted well depth is 647(7), 653(7), and 649(11) cm^{-1}, respectively, for the potentials corresponding to Figs. 4A-4C. The tunneling dynamics of the complex involve mostly planar configurations, motion on R, θ_1, and θ_2 coordinates. At R = 3.97 Å the barrier height for interconversion of the two hydrogen atoms is predicted to be 337(8), 336(8), 337(12) cm^{-1}, for the potentials corresponding to Figs. 4A-4C, respectively.

6. Conclusions

The water bending vibrational spectrum in OC-H_2O complex has been recorded using a supersonic jet mode-hop free quantum cascade laser spectrometer at 6.2 μm. Completely rovibrationally resolved transitions associated with the complex have been observed for both *a*-type and *b*-type transitions. The water tunneling frequency in the ground and excited vibrational states have been analyzed and show a weakening of the intermolecular bond as noted previously [5].

Compound-model morphing methodologies have been radically reformulated to take into consideration the non-linear water molecule. This is an important and critical point in the extension and further development of potential morphing. The methodology of potential morphing can now be applied to any dimer complex comprised of a non-linear and a linear molecule. In addition, it is now feasible to extend the methodology for studying pairwise complexes of non-linear molecules. The generated morphed potentials for OC-H_2O complex allow the modeling of the rovibrational dynamics and prediction of accurate intermolecular rovibrational frequencies of OC-H_2O.

7. Acknowledgements

We give special thanks to The Robert A Welch Foundation (Grant A747) for financial support in the form of post-doctoral fellowship for Blake A. McElmurry and Luis A. Rivera-Rivera, and pre-doctoral fellowship for Sean D. Springer and Kevin W. Scott. In addition, we thank LST/ST, the Laboratory for Molecular Simulation, and the High Performance Research Computing at Texas A&M University.

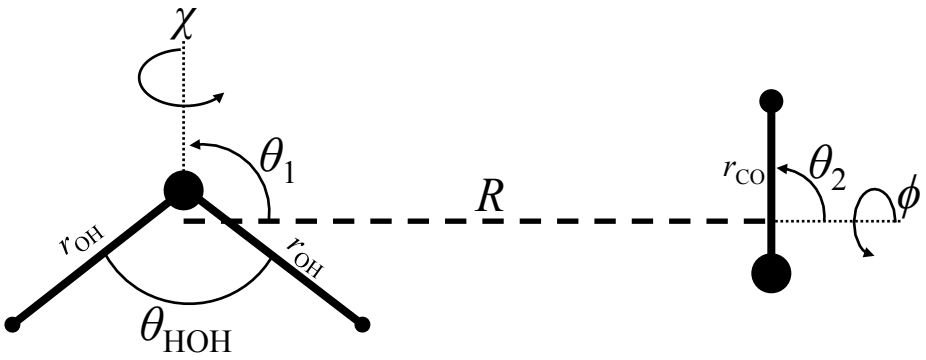

Figure 1. Coordinates system use in this work for OC-H_2O complex.

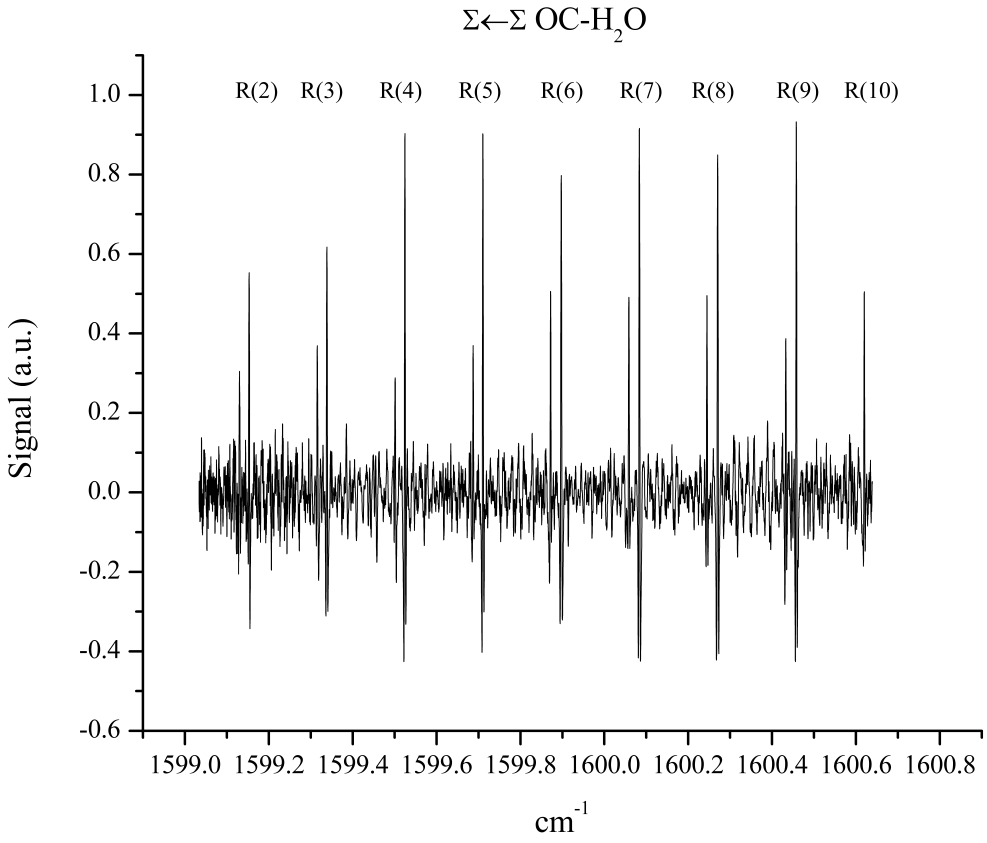

Figure 2. QCL cw supersonic jet spectrum of a segment of the Σ←Σ transition in OC-H_2O.

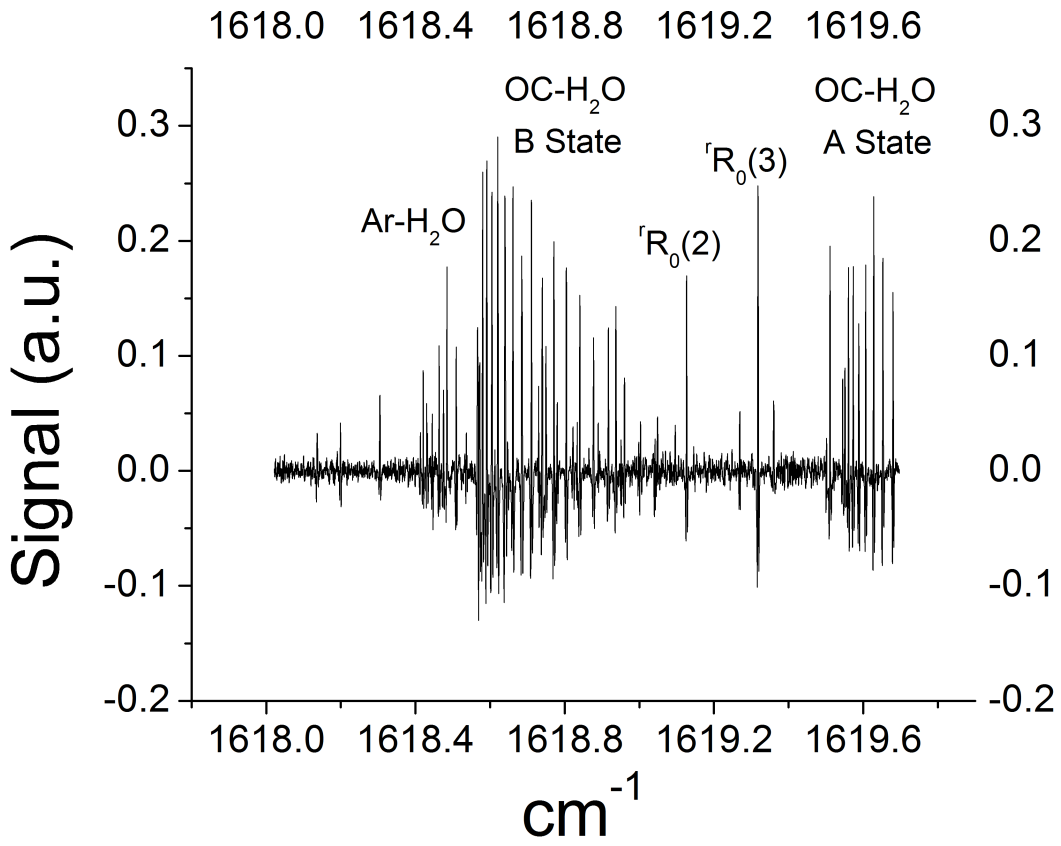

Figure 3. QCL cw supersonic jet spectrum of a segment of the Π←Σ transition in OC-H_2O. Ar-H_2O is present due to the argon expansion.

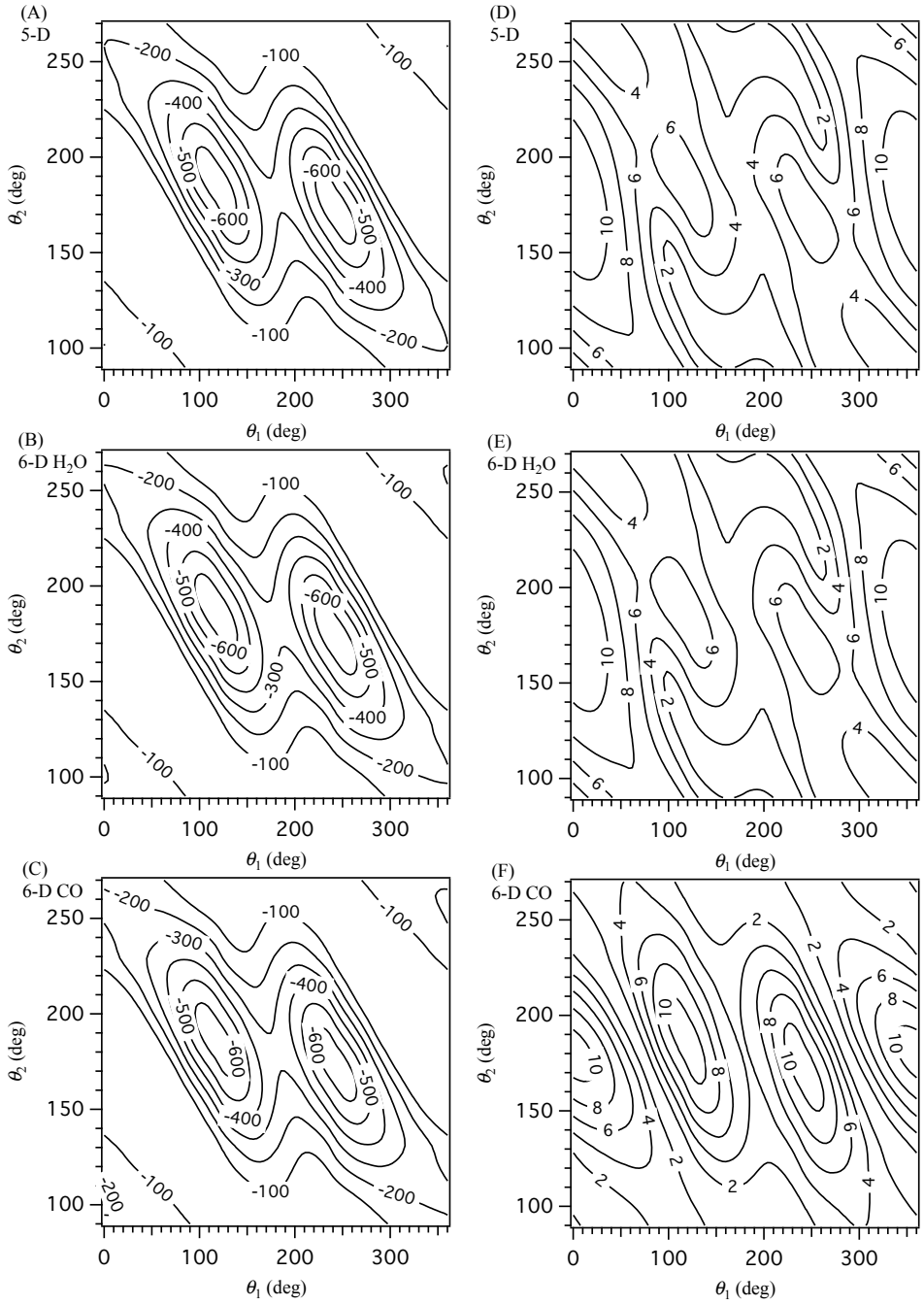

Figure 4. 2-D slices of the CMM-RC interaction potentials of OC-H_2O are shown in Panels A-C. The corresponding estimated errors relative to the potential at infinite separation are shown in Panels D-F. Panels A and D correspond to the 5-D frozen monomer CMM-RC potential. Panels B and E correspond to the adiabatic 6-D CMM-RC potential in the vibrational ground state of the water bending. Panels C and F correspond to the adiabatic 6-D CMM-RC potential in the vibrational ground state of the CO stretching. In all Panels R = 3.97 Å and $\phi = \chi = 0.0°$. The coordinates used are defined in Fig. 1. All contours are in cm^{-1}.

Table I. Character table of the G_4 symmetry group of OC-H_2O.

	E	(12)	E^*	(12)*
Eq. Rotn[a]	E	E	$C_2(y)$	$C_2(y)$
A^+	+1	+1	+1	+1
B^+	+1	-1	+1	-1
A^-	+1	+1	-1	-1
B^-	+1	-1	-1	+1

[a]In this line the effects of the symmetry operations on the Euler angles are described using equivalent rotations [58].

Table II. Matrix elements of the Hamiltonian submatrices corresponding to G_4 symmetry species.

Rot. Symmetry	Overall[a] Symmetry	Matrix element[b]
A'	A^+	$H_{JK';JK''} + H_{1JK';3JK''}$
A'	B^+	$H_{JK';JK''} - H_{1JK';3JK''}$
A''	A^-	$H_{JK';JK''} + H_{1JK';3JK''}$
A''	B^-	$H_{JK';JK''} - H_{1JK';3JK''}$

[a] The G_4 symmetry species of the symmetry adapted wave function is given.
[b] In the body of the table, $H_{JK';JK''}$ stands for the rotational matrix element $< JK'\alpha'|H_R|JK"\alpha" >$ of the rotational Hamiltonian and $H_{1JK';3JK''}$ is defined in Eq. (15).

Table III. Observed $K = 0 \leftarrow 0$ transitions of OC-H_2O in cm^{-1}.

	A State		B State	
J	*P*(*J*)	*R*(*J*)	*P*(*J*)	*R*(*J*)
0				1598.78370
1		1598.94689	1598.41655	
2	1598.21404	1599.13032	1598.23280	1599.15308
3	1598.03173	1599.31583	1598.05033	1599.33848
4	1597.85019	1599.49933	1597.86831	1599.52467
5	1597.66985	1599.68739	1597.68740	1599.71057
6	1597.49008	1599.87193	1597.50636	1599.89734
7	1597.31030	1600.05855	1597.32580	1600.08355
8		1600.24492	1597.14613	1600.27048
9	1596.95347	1600.43286	1596.96761	1600.45794
10	1596.77470	1600.61993	1596.78844	
11	1596.59780	1600.80759	1596.61115	1600.83319
12	1596.42093	1600.99644	1596.43423	1601.02200
13		1601.18511	1596.25800	
14		1601.3733	1596.08146	1601.39953
15		1601.56204	1595.90653	1601.58845
16		1601.75054	1595.73171	1601.77827
17		1601.93915		1601.96672
18			1595.3855	1602.15545
19				1602.34414
20			1595.0393	

Table IV. Observed $K = 0 \leftarrow 1$ transitions of OC-H_2O in cm^{-1}.[a]

	A State			B State		
J	*Q*(*J*)	*P*(*J*)	*R*(*J*)	*Q*(*J*)	*P*(*J*)	*R*(*J*)
0						1619.72691
1	1618.56654		1618.93715	1619.54449		1619.91558
2	1618.57181	1618.19890		1619.55129		1620.10415
3	1618.58010	1618.02025		1619.56063	1618.99817	1620.29765
4	1618.59100	1617.84264	1619.51101	1619.57336	1618.82099	1620.49130
5	1618.60494	1617.66764	1619.70579	1619.58817	1618.64680	1620.68637
6	1618.62071	1617.49466	1619.90368	1619.60674	1618.47481	1620.88502
7	1618.64092		1620.10100	1619.62809	1618.30444	1621.08610
8	1618.66124		1620.30265	1619.65278	1618.13647	1621.28853
9	1618.68506		1620.50445	1619.67980	1617.97091	1621.49277
10	1618.71081		1620.70752		1617.80823	1621.69803
11	1618.73989		1620.91300		1617.64720	1621.90497
12	1618.77094		1621.12017			1622.11393
13	1618.80436					1622.32547
14	1618.84046					
15	1618.87713					
16	1618.91707					
17	1618.96008					

[a]Uncertain whether transitions listed are in fact $K = 0 \leftarrow 1$ or excitation of the intermolecular bend.

Table V. Spectroscopic constants $K = 0 \leftarrow 0$ in cm^{-1}.

	A State		B State	
	Ground	Excited	Ground	Excited
Origin		1598.57892(19)		1598.59956(16)
B	0.091415(17)	0.091671(16)	0.0917527(87)	0.0919971(88)
$D_J \times 10^{-7}$	4.7029924(9)	5.2917146(7)	6.9584582(2)	7.2712021(2)

Table VI. Spectroscopic constants $K = 0 \leftarrow 1$ in cm^{-1}.[a]

	A State	B State
Origin	1618.65688(49)	1619.63466(51)
B	0.092889(13)	0.093077(16)
$D_J \times 10^{-7}$	9.54(63)	9.16(85)
$q \times 10^{-4}$	-3.443(61)	-4.53(12)

[a]Uncertain whether transitions listed are in fact $K = 0 \leftarrow 1$ or excitation of the intermolecular bend.

Table VII. OC-H_2O spectroscopic parameters.[a]

	Excited	Ground
h_3	-0.19694(33)	-0.2782393(26)
θ_3	-	0.0275(14)
h_{3K}	-0.01344(40)	-
$h_{3J} \times 10^3$	-0.0571(49)	-0.0755(53)
$h_{3KJ} \times 10^3$	-0.0363(34)	-0.03574(14)
$h_{3JJ} \times 10^6$	-0.03(14)	-0.0268(43)
$f_3 \times 10^3$	0.0478(19)	0.0564(26)
$f_{3J} \times 10^6$	-	0.0271(32)
ν	1598.6810(3)	-
A	20.46392(50)	19.277226(13)
B	0.092383(19)	0.09209971(15)
C	0.091557(19)	0.09135137(40)
$D_{kj} \times 10^3$	1.013(11)	0.75664(21)
$D_{jj} \times 10^6$	-0.712(15)	-0.68032(47)
$d_1 \times 10^6$	0.071(99)	0.0281(11)
$H_{kjj} \times 10^6$	-0.193(52)	-0.13169(43)
$h_1 \times 10^9$	-0.19(27)	-0.0177(55)

[a]Spectroscopic parameters are in cm^{-1} except θ_3 which is in radians.

Table VIII. Experimental data used in the 5-D CMM-RC fit and fitted values with the uncertainties (σ).

Observable[a]	Isotopomer	Tunneling State	$\left(V^{(0)}_{\text{5D,CMM-RC}}\right)$	$\left(V^{(5)}_{\text{5D,CMM-RC}}\right)$	Exp.	σ
$\overline{B}_0 \times 10^{-2}$	OC-H_2O	A	9.115	9.171	9.170111(7)[b]	0.001
A_0	OC-H_2O	A	18.84	19.83	19.833730(3)[c]	0.01
$D_0 \times 10^{-8}$	OC-H_2O	A	72.0	68.4	69.7(7)[b]	1.0
$\overline{B}_0 \times 10^{-2}$	OC-H_2O	B	9.121	9.175	9.174707(3)[b]	0.001
A_0	OC-H_2O	B	17.77	18.72	18.720718(4)[c]	0.01
$D_0 \times 10^{-8}$	OC-H_2O	B	72.0	68.3	68.4(3)[b]	1.0
$\overline{B}_0 \times 10^{-2}$	OC-D_2O	A	8.685	8.736	8.73678(1)[b]	0.001
A_0	OC-D_2O	A	11.44	11.72	11.78376(2)[c]	0.05
$D_0 \times 10^{-8}$	OC-D_2O	A	56.7	54.9	55.0(10)[b]	1.0
$\overline{B}_0 \times 10^{-2}$	OC-D_2O	B	8.684	8.735	8.73583(1)[b]	0.001
A_0	OC-D_2O	B	11.37	11.65	11.716189(7)[c]	0.05
$D_0 \times 10^{-8}$	OC-D_2O	B	56.7	54.9	52.0(10)[b]	1.0
RMS			50.4	1.2		

[a] Spectroscopic parameters are in cm^{-1}. $\overline{B} = (B+C)/2$
[b] Form Reference [3].
[c] From Reference [4].

Table IX. Experimental data used in the 6-D water bending CMM-RC fit and fitted values with the uncertainties (σ).

Observable[a]	Isotopomer	Tunneling State	$\left(V^{(0)}_{\text{6-D,HOH,CMM-RC}}\right)$	$\left(V^{(5)}_{\text{6-D,HOH,CMM-RC}}\right)$	Exp.	σ
$\overline{B}_0 \times 10^{-2}$	OC-H_2O	A	9.114	9.171	9.170111(7)[b]	0.001
A_0	OC-H_2O	A	18.86	19.83	19.833730(3)[c]	0.01
$D_0 \times 10^{-8}$	OC-H_2O	A	72.3	68.3	69.7(7)[b]	1.0
$\overline{B}_0 \times 10^{-2}$	OC-H_2O	B	9.120	9.175	9.174707(3)[b]	0.001
A_0	OC-H_2O	B	17.76	18.72	18.720718(4)[c]	0.01
$D_0 \times 10^{-8}$	OC-H_2O	B	72.2	68.2	68.4(3)[b]	1.0
$\overline{B}_0 \times 10^{-2}$	OC-D_2O	A	8.685	8.736	8.73678(1)[b]	0.001
A_0	OC-D_2O	A	11.44	11.71	11.78376(2)[c]	0.05
$D_0 \times 10^{-8}$	OC-D_2O	A	56.7	54.9	55.0(10)[b]	1.0
$\overline{B}_0 \times 10^{-2}$	OC-D_2O	B	8.684	8.735	8.73583(1)[b]	0.001
A_0	OC-D_2O	B	11.37	11.65	11.716189(7)[c]	0.05
$D_0 \times 10^{-8}$	OC-D_2O	B	56.9	54.9	52.0(10)[b]	1.0
RMS			50.3	1.2		

[a] Spectroscopic parameters are in cm^{-1}. $\overline{B} = (B+C)/2$
[b] Form Reference [3].
[c] From Reference [4].

Table X. Experimental data used in the 6-D CO stretching CMM-RC fit and fitted values with the uncertainties (σ).

Observable[a]	Isotopomer	Tunneling State	$\left(V^{(0)}_{\text{6-D,CO,CMM-RC}}\right)$	$\left(V^{(5)}_{\text{6-D,CO,CMM-RC}}\right)$	Exp.	σ
$\overline{B}_0 \times 10^{-2}$	OC-H_2O	A	9.102	9.171	9.170111(7)[b]	0.001
A_0	OC-H_2O	A	18.80	19.82	19.833730(3)[c]	0.01
$D_0 \times 10^{-8}$	OC-H_2O	A	73.2	68.9	69.7(7)[b]	1.0
$\overline{B}_0 \times 10^{-2}$	OC-H_2O	B	9.108	9.175	9.174707(3)[b]	0.001
A_0	OC-H_2O	B	17.73	18.73	18.720718(4)[c]	0.01
$D_0 \times 10^{-8}$	OC-H_2O	B	73.1	68.9	68.4(3)[b]	1.0
$\overline{B}_0 \times 10^{-2}$	OC-D_2O	A	8.673	8.734	8.73678(1)[b]	0.001
A_0	OC-D_2O	A	11.44	11.73	11.78376(2)[c]	0.05
$D_0 \times 10^{-8}$	OC-D_2O	A	57.5	55.3	55.0(10)[b]	1.0
$\overline{B}_0 \times 10^{-2}$	OC-D_2O	B	8.672	8.733	8.73583(1)[b]	0.001
A_0	OC-D_2O	B	11.37	11.67	11.716189(7)[c]	0.05
$D_0 \times 10^{-8}$	OC-D_2O	B	57.5	55.3	52.0(10)[b]	1.0
ν_3	OC-H_2O	A	2153.13	2153.61	2153.5953(1)[d]	0.01
$\overline{B}_3 \times 10^{-2}$	OC-H_2O	A	9.060	9.128	9.12459(23)[d]	0.001
$D_3 \times 10^{-8}$	OC-H_2O	A	75.3	70.4	72.2(9)[d]	1.0
ν_3	OC-H_2O	B	2153.17	2153.65	2153.6478(1)[d]	0.01
$\overline{B}_3 \times 10^{-2}$	OC-H_2O	B	9.067	9.132	9.12971(19)[d]	0.001
$D_3 \times 10^{-8}$	OC-H_2O	B	75.2	70.3	69.8(5)[d]	1.0
ν_3	OC-D_2O	A	2154.06	2154.53	2154.5375(1)[d]	0.01
$\overline{B}_3 \times 10^{-2}$	OC-D_2O	A	8.633	8.692	8.69305(19)[d]	0.001
$D_3 \times 10^{-8}$	OC-D_2O	A	58.8	56.2	55.1(8)[d]	1.0
ν_3	OC-D_2O	B	2154.07	2154.53	2154.5409(1)[d]	0.01
$\overline{B}_3 \times 10^{-2}$	OC-D_2O	B	8.632	8.691	8.69217(21)[d]	0.001
$D_3 \times 10^{-8}$	OC-D_2O	B	58.8	56.2	53.1(10)[d]	1.0
RMS			50.9	1.8		

[a] Spectroscopic parameters are in cm^{-1}. $\overline{B} = (B+C)/2$
[b] Form Reference [3]. [c] From Reference [4]. [d] From Reference [5].

Table XI. Optimized values for the morphing parameters for OC-H_2O.

α	$C_\alpha^{(0)}$	$\left(V^{(5)}_{\text{5D,CMM-RC}}\right)$	$\left(V^{(5)}_{\text{6-D,HOH,CMM-RC}}\right)$	$\left(V^{(5)}_{\text{6-D,CO,CMM-RC}}\right)$
1	1.0	0.9449(64)	0.9569(65)	0.9691(27)
2	0.0	-0.4257(40)	-0.4220(40)	-0.4310(35)
3	1.0	0.888(69)	0.900(70)	1.083(17)
4	1.0	0.9736(50)	0.9687(50)	0.9664(33)
5	0.0	-0.00144(23)	-0.00144(23)	-0.000315(94)

Table XII. Prediction of the water bending in OC-H_2O complex, based on the 6-D water bending CMM-RC potential $\left(V^{(5)}_{\text{6-D,HOH,CMM-RC}}\right)$ with and without corrections for the kinetic energy (KE) of the water monomer.[a]

Observable[b]	Isotopomer	Without KE Correction	With KE Correction	Exp.
ν_5 (OC-H_2O)	OC-H_2O	1597.69	1598.68	1598.6810(3)[c]
$\overline{B}_5 \times 10^{-2}$	OC-H_2O	9.173	9.197	9.1970(19)[c]
A_5	OC-H_2O	20.51	20.79	20.46392(50)[c]
ν_5 (OC-D_2O)	OC-D_2O	1180.11	1180.62	1180.6198(2)[d]
$\overline{B}_5 \times 10^{-2}$	OC-D_2O	8.736	8.755	8.754(1)[d]
A_5	OC-D_2O	12.28	12.44	12.4516(3)[d]

[a] Spectroscopic parameters are in cm^{-1}. $\overline{B} = (B+C)/2$
[b] This data was not included in the fitting but was predicted using the final morphed potential, which include corrections to the kinetic energy of the water monomer. See text for details.
[c] This work.
[d] From Reference [62].

Table XIII. Predicted fundamental intermolecular vibrational frequencies (in cm^{-1}) for OC-H_2O.[a]

	$\left(V^{(5)}_{\text{5D,CMM-RC}}\right)$	$\left(V^{(5)}_{\text{6-D,HOH,CMM-RC}}\right)$	$\left(V^{(5)}_{\text{6-D,CO,CMM-RC}}\right)$
ν_9	19.75, 18.63	19.74, 18.63	19.73, 18.64
ν_8	50.55, 48.74	50.79, 48.97	50.57, 48.76
ν_4	78.32, 78.58	78.50, 78.75	78.49, 78.76

[a] The first frequency value correspond to the A tunneling state and the second frequency value correspond to the B tunneling state. See text for description of the intermolecular vibrations.

Table XIV. Predicted values for D_0 energies for OC-H_2O and OC-D_2O.

	D_0 (cm^{-1}) OC-H_2O	D_0 (cm^{-1}) OC-D_2O
$\left(V^{(5)}_{\text{5D,CMM-RC}}\right)$	337(5)	389(6)
$\left(V^{(5)}_{\text{6-D,HOH,CMM-RC}}\right)$	342(5)	394(6)
$\left(V^{(5)}_{\text{6-D,CO,CMM-RC}}\right)$	339(5)	391(6)

References

[1] A. A. Vigasin, Z. Slanina (Eds.), Molecular Complexes in Earth's, Planetary, Cometary, and Interstellar Atmospheres, World Scientific, Singapore, 1998.

[2] A. M. Shaw, Astrochemistry: From Astronomy to Astrobiology, Wiley, Chichester, 2006.

[3] D. Yaron, K. I. Peterson, D. Zolandz, W. Klemperer, F. J. Lovas, R. D. Suenram, J. Chem. Phys. 92 (1990) 7095.

[4] R. E. Bumgarner, S. Suzuki, P. A. Stockman, P. G. Green, G. A. Blake, Chem. Phys. Lett. 176 (1991) 123.

[5] M. D. Brookes, A. R. W. McKellar, J. Chem. Phys. 109 (1998) 5823.

[6] L. Oudejans, R. E. Miller, Chem. Phys. Lett. 306 (1999) 214.

[7] T.-L. Tso, E. K. C. Lee, J. Phys. Chem. 89 (1985) 1612, and references contained therein.

[8] A. Givan, A. Loewenschuss, C. J. Nielsen, J. Chem. Soc. Faraday Trans. 92 (1996) 4927, and references contained therein.

[9] S. Chin, T. A. Ford, W. B. Person, J. Mol. Struct. 113 (1984) 341.

[10] A. E. Reed, F. Weinhold, L. A. Curtiss, D. J. Pochatko, J. Chem. Phys. 84 (1986) 5687.

[11] T. D. Mokomela, I. Rencken, G. A. Yeo, T. A. Ford, J. Mol. Struct. 275 (1992) 33.

[12] C. A. Parish, J. D. Augspurger, C. E. Dykstra, J. Phys. Chem. 96 (1992) 2069.

[13] J. Lundell, J. Phys. Chem. 99 (1995) 14290.

[14] J. Lundell, Z. Latajka, J. Phys. Chem. A 101 (1997) 5004.

[15] J. Langlet, J. Caillet, M. Allavena, J. Mol. Struct. 450 (1998) 69.

[16] J. Sadlej, V. Buch, J. Chem. Phys. 100 (1994) 4272.

[17] J. Sadlej, B. Rowland, J. P. Devlin, V. Buch, J. Chem. Phys. 102 (1995) 4804.

[18] P. Sandler, J. Sadlej, T. Feldmann, V. Buch, J. Chem. Phys. 107 (1997) 5022.

[19] S. D. Springer, B. A. McElmurry, Z. Wang, I. I. Leonov, R. R. Lucchese, J. W. Bevan, L. H. Coudert, Chem. Phys. Lett. 633 (2015) 229.

[20] L. A. Rivera-Rivera, B. A. McElmurry, Z. Wang, I. I. Leonov, R. R. Lucchese, J. W. Bevan, Chem. Phys. Lett. 522 (2012) 17.

[21] A. McIntosh, Z. Wang, J. Castillo-Chará, R. R. Lucchese, J. W. Bevan, R. D. Suenram, A. C. Legon, J. Chem. Phys. 111 (1999) 5764.

[22] L. A. Rivera-Rivera, R. R. Lucchese, J. W. Bevan, Phys. Chem. Chem. Phys. 12 (2010) 7258.

[23] L. A. Rivera-Rivera, Z. Wang, B. A. McElmurry, F. F. Willaert, R. R. Lucchese, J. W. Bevan, R. D. Suenram, F. J. Lovas, J. Chem. Phys. 133 (2010) 184305.

[24] Z. Wang, B. A. McElmurry, R. R. Lucchese, J. W. Bevan, L. H. Coudert, J. Chem. Phys. 134 (2011) 064317.

[25] L. A. Rivera-Rivera, Z. Wang, B. A. McElmurry, R. R. Lucchese, J. W. Bevan, G. Kanschat, Chem. Phys. 390 (2011) 42.

[26] L. A. Rivera-Rivera, B. A. McElmurry, K. W. Scott, R. R. Lucchese, J. W. Bevan, J. Phys. Chem. A 117 (2013) 8477.

[27] A. L. McIntosh, Z. Wang, R. R. Lucchese, J. W. Bevan, Infrared Phys. Technol. 45 (2004) 301.

[28] B. A. McElmurry, L. A. Rivera-Rivera, K. W. Scott, Z. Wang, I. I. Leonov, R. R. Lucchese, J. W. Bevan, Chem. Phys. 409 (2012) 1.

[29] H.-J. Werner, P. J. Knowles, R. Lindh, F. R. Manby, M. Schütz, P. Celani, T. Korona, A. Mitrushenkov, G. Rauhut, T. B. Adler, R. D. Amos, A. Bernhardsson, A. Berning, D. L. Cooper, M. J. O. Deegan, A. J. Dobbyn, F. Eckert, E. Goll, C. Hampel, G. Hetzer, T. Hrenar, G. Knizia, C. Köppl, Y. Liu, A. W. Lloyd, R. A. Mata, A. J. May, S. J. McNicholas, W. Meyer, M. E. Mura, A. Nicklass, P. Palmieri, K. Pflüger, R. Pitzer, M. Reiher, U. Schumann, H. Stoll, A. J. Stone, R. Tarroni, T. Thorsteinsson, M. Wang, A. Wolf, MOLPRO, version 2010.1, a package of ab initio programs, Cardiff, UK, 2010.

[30] T. H. Dunning, J. Chem. Phys. 90 (1989) 1007.

[31] D. E. Woon, T. H. Dunning, J. Chem. Phys. 98 (1993) 1358.

[32] T. H. Dunning, K. A. Peterson, A. K. Wilson, J. Chem. Phys. 114 (2001) 9244.

[33] S. F. Boys, F. Bernardi, Mol. Phys. 19 (1970) 553.

[34] S. V. Shirin, N. F. Zobov, R. I. Ovsyannikov, O. L. Polyansky, J. Tennyson, J. Chem. Phys. 128 (2008) 224306.

[35] A. W. Mantz, J. K. G. Watson, K. N. Rao, D. L. Albritto, A. L. Schmelte, R. N. Zare, J. Mol. Spectrosc. 39 (1971) 180.

[36] R. Sankari, M. Ehara, H. Nakatsuji, Y. Senba, K. Hosokawa, H. Yoshida, A. De Fanis, Y. Tamenori, S. Aksela, K. Ueda, Chem. Phys. Lett. 380 (2003) 647.

[37] A. van der Avoird, P. Wormer, F. Mulder, R. Berns, Top. Curr. Chem. 93 (1980) 1.

[38] A. van der Avoird, P. E. S. Wormer, R. Moszynski, Chem. Rev. 94 (1994) 1931.

[39] A. van der Avoird, D. J. Nesbitt, J. Chem. Phys. 134 (2011) 044314.

[40] P. Lancaster, K. Šalkauskas, Curve and surface fitting: An introduction, Academic Press, London, 1986.

[41] T.-S. Ho, H. Rabitz, J. Chem. Phys. 104 (1996) 2584.

[42] J. Castillo-Chará, R. R. Lucchese, J. W. Bevan, J. Chem. Phys. 115 (2001) 899.

[43] J. M. Bowman, Acc. Chem. Res. 19 (1986) 202.

[44] J. W. Cooley, Math. Comp. 15 (1961) 363.

[45] H. Wei, T. Carrington, Jr., J. Chem. Phys. 97 (1992) 3029.

[46] W. H. Press, B. P. Flannery, S. A. Teukolsky, W. T. Vetterling, Numerical recipes; the art of scientific computing, Cambridge University Press, Cambridge, 1986.

[47] G. Brocks, A. van der Avoird, B. T. Sutcliffe, J. Tennyson, Mol. Phys. 50 (1983) 1025.

[48] C. Leforestier, L. B. Braly, K. Liu, M. J. Elrod, R. J. Saykally, J. Chem. Phys. 106 (1997) 8527.

[49] J. Castillo-Chará, J. W. Bevan, R. R. Lucchese, Comput. Phys. Commun. 145 (2002) 48.

[50] J. Castillo-Chará, R. R. Lucchese, J. W. Bevan, J. Chem. Phys. 115 (2001) 899.

[51] J. K. Cullum, R. A. Willoughby, Lanczos algorithms for large symmetric eigenvalue computations, Birkhäuser, Boston, 1985.

[52] J. A. Coxon, P. G. Hajigeorgiou, J. Chem. Phys. 121 (2004) 2992.

[53] F. C. De Lucia, P. Helminger, R. L. Cook, W. Gordy, Phys. Rev. A 5 (1972) 487.

[54] J. K. Messer, F. C. De Lucia, P. Helminger J. Mol. Spectrosc. 105 (1984) 139.

[55] C. Camy-Peyret, J.-M. Flaud, Mol. Phys. 32 (1976) 523.

[56] C. Camy-Peyret, J.-M. Flaud, A. Mahmoudi, G. Guelachvili, J. W. C. Johns, Int. J. Infrared Milli. 6 (1985) 199.

[57] H. O. Leung, M. D. Marshall, R. D. Suenram, F. J. Lovas, J. Chem. Phys. 90 (1989) 700.

[58] P. R. Bunker, Molecular Symmetry and Spectroscopy, 1st ed., Academic Press, New York, 1979.

[59] L. H. Coudert, J. T. Hougen, J. Mol. Spectrosc. 130 (1988) 86.

[60] L. H. Coudert, K. Matsumura, F. J. Lovas, J. Mol. Spectrosc. 147 (1991) 46.

[61] J. T. Hougen, J. Mol. Spectrosc. 114 (1985) 395.

[62] Y. Zhu, R. Zheng, S. Li, Y. Yang, C. Duan, J. Chem. Phys. 139 (2013) 214309.